Trans. of the Society of Instrument and Control Engineers
Vol.E-2, No.1, 64/71 (2002)

An Automated Registration Technique for Remotely Sensed Images by Using Spatial Correlation between Local Triangles†

Hiroshi HANAIZUMI*, Hiroshi OKUMURA**,
Hiroe TSUBAKI*** and Sadao FUJIMURA****

Remotely sensed images have different geometrical distortion caused by change of orbits or posture of platforms. Precise registration of these images is very important in multi-temporal processing. There have been reported a lot of registration methods for multi-temporal processing of images. These methods require ground control point (GCP) pairs for describing the relative geometrical discrepancy between images, and for determining the coordinate transfer function from one to another. Selection of GCP pairs is essential in these methods. It is, however, difficult and time consuming to select them precisely. Inadequate selection of them causes registration error.

For reduction of error in registration and time for selecting GCP pairs, we propose an automated registration technique (ART). In this technique, we assume that only small change occurs in the scene during the period between the first and the second sensing. The proposed technique ART consists of three stages of processing, that is, taking initial GCP pairs, detection and division, and local Affine transformation (ATF).

In the first stage, we take three GCP pairs on both images for making initial triangles T_1 and T_2. In the second stage, residual discrepancy after ATF of T_2 onto T_1 is evaluated in the detection procedure. We use spatial correlation as a key for measuring discrepancy in the sense of spatial structure. If the residual discrepancy is detected, T_1 and T_2 are divided into two sub-triangles, respectively. These procedures are iteratively applied to the triangles until the geometrical distortion between the images is sufficiently corrected by local ATF. The third stage of ART is application of local ATF to each triangle pair.

In this paper, we describe the principle and the procedure used in the proposed technique. The validity of the technique is confirmed by numerical simulation and application to actual airborne images.

Key Words: automated registration, spatial correlation, area division, local Affine transformation, geometrical distortion

1. INTRODUCTION

Most remotely sensed images are geometrically distorted due to change of platform orbit and/or attitude. Especially, airborne sensor images often have severe distortion. In order to detect temporal change from multi-temporal images, we have to register them accurately so that pixels with the same address (line and column) correspond to the same terrain point. There have been proposed many methods for image registration [1)~11)]. Most of them the registration was performed by two steps; determination of coordinate transfer function from selected ground control point (GCP) pairs, and moving position of all pixels using the function. For achieving highly accurate registration,.it was required to select many GCP pairs uniformly over the image [12), 13)], and to adopt the optimal transfer function [14)]. It is, however, very time consuming operation to select many GCP pairs manually, and very difficult both to keep their spatial uniformity [15)] and to estimate the optimal transfer function. In most case, poor performances were often obtained after very time consuming operations. Therefore, algorithms have been proposed for automated selection of GCP pairs [16)] or for automated registration in which center of an area extracted by an spatial segmentation method was regarded as the GCP [17)]. These methods were effective in removing geometrical disparities which were described by a linear function. In this paper, we propose an Automated Registration Technique (ART) which well removes severe disparities in airborne remote sensing images only from three initial GCP pairs [18)~21)]. In this technique, Affine transformation (ATF) is applied to triangle areas determined by the initial GCP pairs. Then residual discrepancy is

† Presented in the 14^{th}SICE Remote Sensing Symposium (Oct. 1998)

* Faculty of Engineering, Hosei University, Koganei
** Remote Sensing & Image Research Center, Chiba University, Chiba
*** Faculty of Science and Engineering, Keio University, Yokohama
**** Faculty of Engineering, University of Tokyo, Bunkyo-ku, Tokyo

(Received April 6, 1992)
(Revised June 26, 1992)

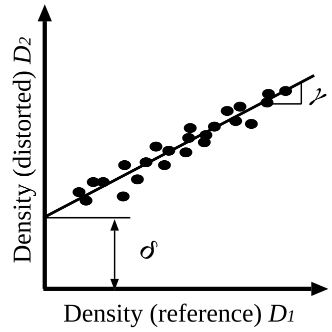

Fig. 1 Density scatter diagram between reference image and distortion image

evaluated. If large discrepancy is detected (i.e. the registration performance is low), new GCP[(1)] pair for binary dividing the initial triangle is automatically searched and generated so that better performance is obtained. These processes are recursively applied to sub-triangles until no more division improves the registration performance. The procedure is very similar with approximating a curve by line segments. ART adopts a hierarchical process [22] in searching new GCP pair, does not need to estimate the optimal transfer function and needs only three initial GCP pairs. Thus, ART has high performance and high efficiency in the image registration.

2. PRINCIPLE

We call one of two images to be registered as "reference image" and the other as "distortion image". The distortion image is registered onto the reference. At the first stage of ART, 3 GCPs and their corresponding points are taken on reference and distortion image, respectively. The triangle area on the distortion image is transformed by ATF onto that on the reference one. After ATF, the residual discrepancy is detected and the triangle area is divided into two sub-triangles when higher performance is obtained by the division. The detection and division procedures are repeatedly applied until division does not improve the performance.

2.1 Detection procedure

We assume that there are few areas with temporal change in the images to be registered. The residual discrepancy after ATF is evaluated by spatial similarity between the reference and the distortion images. The spatial similarity is measured by linearity of the relation between densities D_1 and D_2 in the density scatter diagram (see Fig.1) of pixels in the both triangles.

Spectral reflectance L is usually recorded into pixel densities D_1 and D_2 with linear functions as

$$D_1 = a_1 L + b_1 + \varepsilon_1, \tag{1}$$

$$D_2 = a_2 L + b_2 + \varepsilon_2, \tag{2}$$

respectively. In these equations, $a_i (i = 1, 2)$ and $b_i (i = 1, 2)$ are gain and offset coefficients, respectively, and $\varepsilon_i (i = 1, 2)$ random noises with zero mean. Binding these equations, we obtain a linear relation as

$$\begin{aligned} D_2 &= a_2 a_1^{-1}(D_1 - b_1 - \varepsilon_1) + b_2 + \varepsilon_2 \\ &= \gamma D_1 + \delta + \epsilon. \end{aligned} \tag{3}$$

This suggests density scatter diagram between two images forms line-shaped pattern with minimal dispersion due to random noise is obtained when the two images are perfectly registered. Since larger disparities yield the severer dispersion, we can evaluate how the images are registered from the dispersion. We use the correlation coefficient r of the linear relation shown in the density scatter diagram as a measure for evaluating the dispersion.

$$r = S_{12}(S_{11}S_{22})^{-1/2}, \tag{4}$$

where,

$$S_{km} = \sum_{i=1}^{n}(D_{ki} - \mu_k)(D_{mi} - \mu_m), (k = 1, 2; m = 1, 2). \tag{5}$$

In the equations above, we assume that the density scatter diagram is formed by n pixels, and that μ_1 and μ_2 are mean densities of pixels in both images, respectively. Since the correlation coefficient is independent of gain and offset for image recording, the evaluation of the residual discrepancy between the images is stably performed without affecting the difference of gain and offset.

2.2 Division procedure

In the division procedure, we take 3 GCPs on IMG1 and also 3 GCPs corresponding to them on IMG2. These GCPs determine triangles on IMG1 and on IMG2, respectively. The triangles are iteratively divided into subtriangles until the geometrical discrepancy can be corrected by ATF. In order to divide the triangles, a new GCP is generated on IMG1, and its corresponding GCP is searched on IMG2. For reduction of processing time, candidates for the corresponding GCP are hierarchically selected by local mask search (LMS) and global mask search (GMS). The spatial similarity described above is used as the key for the searches. The triangles are divided when the division increases the spatial similarity.

(1) We refer new corresponding point automatically generated by the algorithm as GCP even though the term GCP is often used for terrain point having special feature such as road cross or edges of a building.

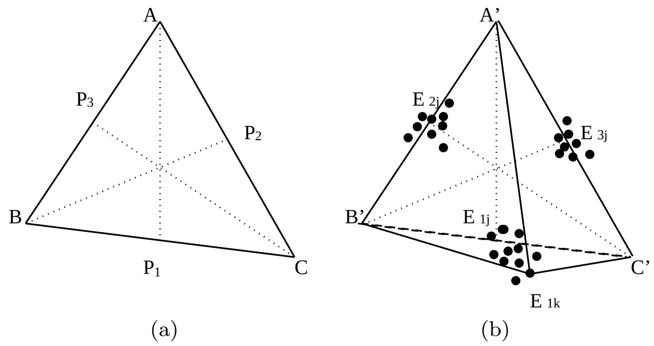

Fig. 2 Candidates for triangle division on the reference image (a) and those on the distortion image (b)

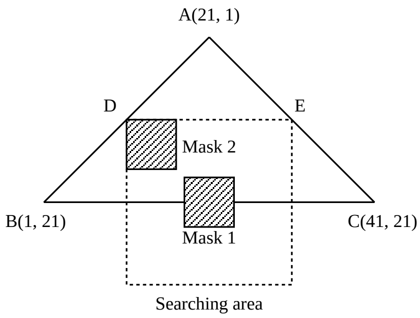

Fig. 3 Template triangle for LMS and GMS

When divided, the same procedure is applied to the sub-triangles. This procedure is continued until the spatial similarity is no more improved, i.e. we stop the procedure when the correlation coefficient of the density scatter diagram for one of the sub-triangles is not larger than that of the original triangle.

3. PROCEDURES

We describe the procedure for generating new GCP pair for the triangle division. We refer one of two images to be registered as IMG1 and IMG2 (IMG2 is registered onto IMG1), and the transformed image (from IMG2) by ATF as IMG3. The detection procedure is applied to IMG1 and IMG3, and when the spatial discrepancy is detected, both IMG1 and IMG2 are divided into sub-triangles, respectively.

3.1 detection of discrepancy

Suppose that $\Delta A'B'C'$ on IMG2 is registered onto ΔABC on IMG1. In the detection procedure, we test whether the division of the triangle improves the spatial similarity, i.e. correlation coefficient derived from the density scatter diagram becomes larger. We take 3 midpoints $P_i(i = 1, 2, 3)$ on the sides $\overline{AB}$, $\overline{BC}$ and $\overline{CA}$, respectively, as shown in Fig.2 (a).

These points are used as candidates of new GCP for the triangle division. The possible corresponding points for the candidates on IMG1 are marked, as shown in Fig.2 (b), by the following Local Mask Search (LMS) and Global Mask Search (GMS). Among these pair of GCP candidates, the best pair is selected so that product of correlation coefficients r_1 and r_2 calculated in the both sub-triangles takes the maximum. When the correlation coefficient estimated in the original triangle r_0 is smaller than both r_1 and r_2, we regard that the spatial discrepancy is detected. The original triangle is then divided into two sub-triangles using the best GCP pair.

3.2 Local Mask Search (LMS)

Candidate points $E_{ij}(i = 1, 2, 3; j = 1, 2, ..., N)$ corresponding to the midpoints $P_i(i = 1, 2, 3)$ of ΔABC in IMG1 are searched around those of $\Delta A'B'C'$ in IMG2. A small mask with size of 3×3 pixels is used for the search. We put mask 1 on $P_i(i = 1, 2, 3)$ and scan the same size mask 2 around the corresponding midpoints. Correlation coefficient derived from the density scatter diagram of pixels in masks 1 and 2 is used as the key for the search. Candidate points providing highest N correlation coefficients are marked for each midpoint on the side of ΔABC. We set $N = 30$ in the following processing.

3.3 Global Mask Search (GMS)

Now, we have $3N$ candidate pairs of GCP for dividing the original triangle. The best GCP pair P_m and $E_{mk}(1 \le m \le 3; 1 \le k \le N)$ is selected among all candidate pairs. Suppose that r_0, r_{1mk} and r_{2mk} are the correlation coefficients derived from the triangle pairs (ΔABC - $\Delta A'B'C'$), (ΔABP_m - $\Delta A'B'E_{mj}$) and (ΔAP_mC - $\Delta A'E_{mj}C'$), respectively. Figure 2(b) shows the example where GCP pair E_{1k} is evaluated.

In order to avoid the complex processing, we generalize the procedures for various size triangles by using a triangle template shown in Fig.3. Both ΔABC and $\Delta A'B'C'$ are transformed onto the template by using ATF. Search area, mask sizes and their scan steps are determined corresponding to the size of the both triangles.

3.4 Actual flow of processing

Figure 4 shows the processing flow of the proposed technique ART. Step by step procedures are listed as follows:

Step 1. Take 3 GCP pairs on both images IMG1 and IMG2. Triangle area determined by the 3 GCPs on IMG2 is registered onto those on IMG1.

Step 2. Obtain IMG3 by ATF transforming IMG2 onto IMG1, and make density scatter diagram from pixels in both triangles on IMG1 and IMG3. Then, derive correlation coefficient r_0 from the density scatter diagram.

Step 3. Generate $3N$ candidate GCPs $E_{ij}(i =$

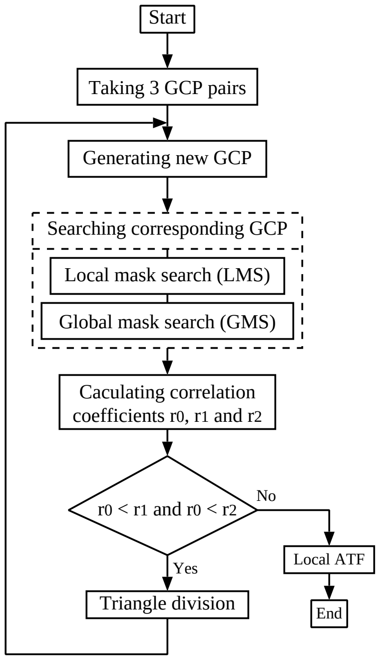

Fig. 4 Flow of processing

$1,2,3; j = 1,2,...,N$) on the side of the triangle on IMG2 corresponding to $P_i (i = 1,2,3)$ on IMG1 by using LMS and GMS.

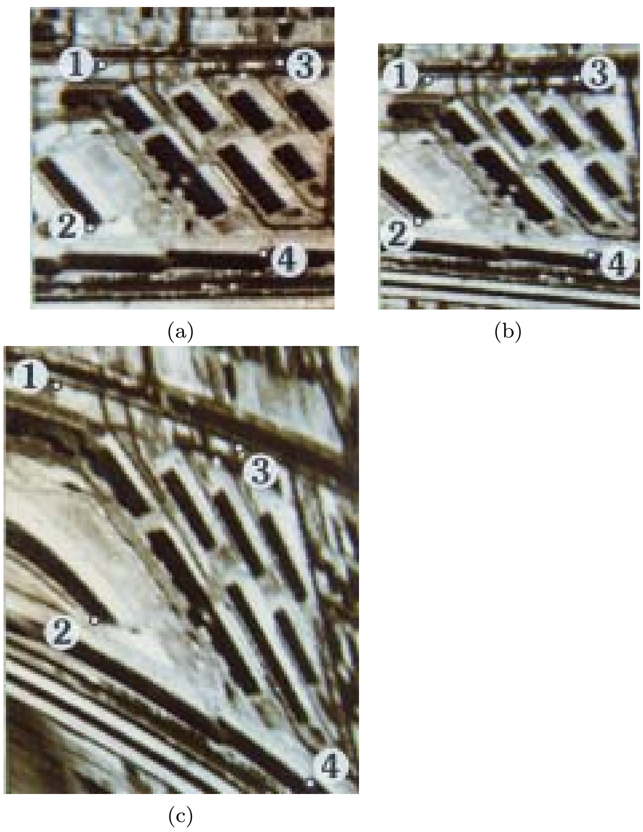

Fig. 5 Reference image IMG-A (a), slightly distorted image IMG-B (b) and severely distorted one IMG-C (c)

Step 4. For every GCP pair P_i and E_{ij}, simulate the division and derive the correlation coefficients r_{1ij} and r_{2ij} from two sub-triangles. Select the best GCP pair P_m and E_{mk} which maximizes the product of the correlation coefficients. When the coefficients for the best GCP pair satisfies the condition of $r_{1mk} > r_0$ and $r_{2mk} > r_0$, we regard as the division improves the registration accuracy. Divide the original triangles into two sub-triangles by using the best GCP pair P_m and E_{mk}.

Step 5. In the two sub-triangles, replace $r_0 \leftarrow r_{1mk}$ and $r_0 \leftarrow r_{2mk}$, respectively, and repeat procedures from Step 3 to Step 5, recursively.

step 6. When the condition in Step 4 is not satisfied, stop the division and apply ATF to current triangles for registering IMG2 onto IMG1.

step 7. When all the triangles are transformed by ATF, save the resultant image and finish all procedures.

4. Numerical Simulation

In order to evaluate the performance of ART, we compare the result processed by ART with that by ATF. An airborne remote sensing data set is used for the simulation. A near infrared band ($0.92 \sim 1.0\mu m$) image with 256×256 pixels in size is cut out as the reference (IMG-A) and another two images (IMG-B and IMG-C) are produced by distorting the reference with the coordinate transfer functions of

$$\begin{cases} X = 0.002U^2 - 0.002UV + 1.03U \\ Y = 0.002V^2 - 0.0015UV + 0.94V \end{cases} \tag{6}$$

and

$$\begin{cases} X = 0.005U^2 - 0.002UV + 0.8U - 0.15V + 15 \\ Y = 0.001V^2 - 0.002UV - 0.2U + 0.6V + 10 \end{cases} \tag{7}$$

We regard the point $(90, 50)$ on IMG1 as the origin of both transfer functions. In these equations, pixel density of a point (U, V) on IMG-B or IMG2 comes from that of the pixel (X, Y) on IMG-A. These images are shown in Fig.5.

In order to make the evaluation easy, we used 4 GCP pairs as the initial GCPs, i.e. two initial triangles. Figures 6 are color composite image where we assign IMG-A to 'Red' and processed result of IMG-B (slightly distorted image) by ART (a) or by ATF (b) to 'Green' and 'Blue'. In the color composite image, black and white region indicates that the images are perfectly registered. On the other hand, the residual discrepancy is indicated as 'red region' or 'bluish region'. The results for the severely distorted image (IMG-C) is shown in Fig.7. Figures 6

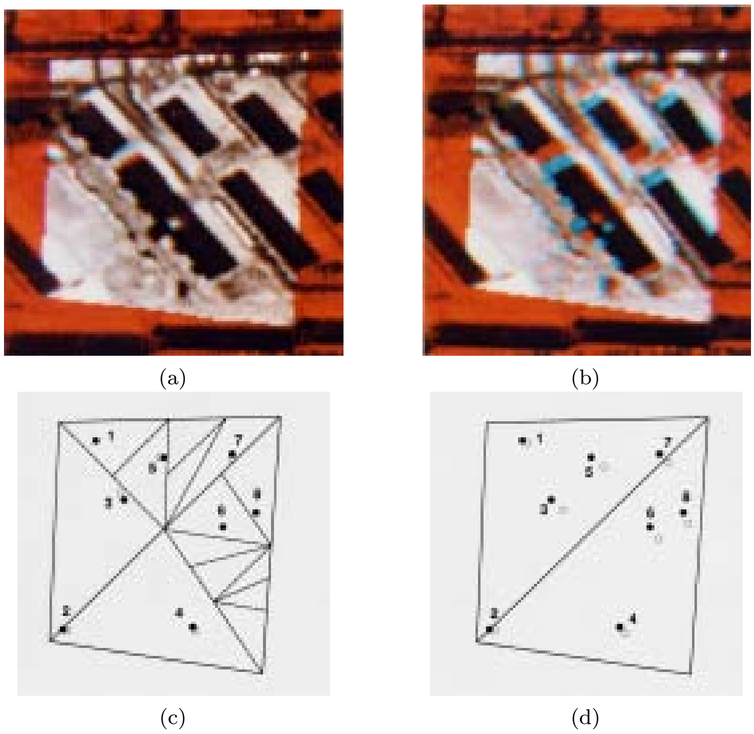

Fig. 6 Simulation results for slightly distorted image; result processed by ART (a) and one by ATF (b), and area divisions on the reference image by ART (c) and by ATF (d)

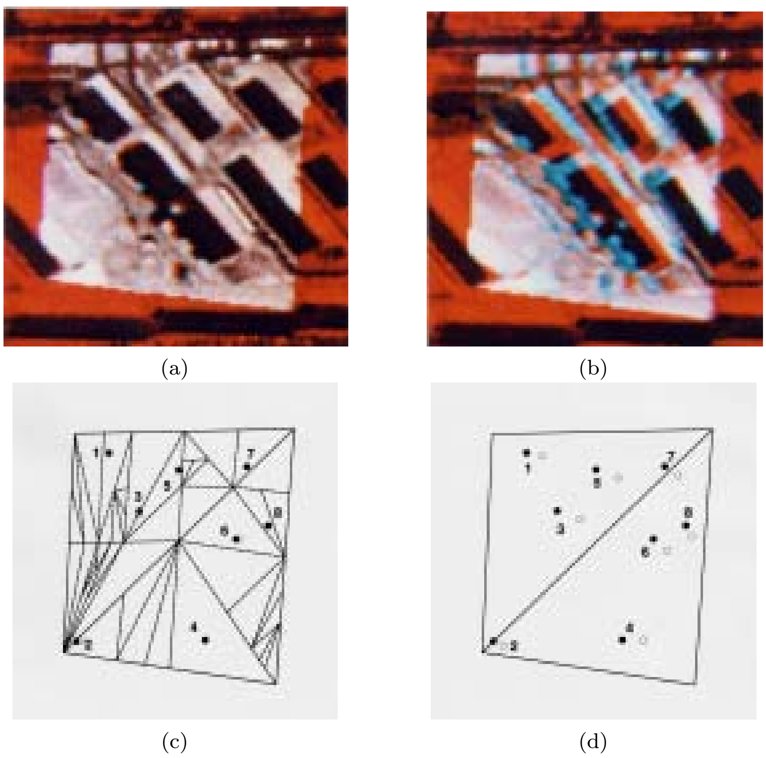

Fig. 7 Simulation results for severely distorted image; result processed by ART (a) and one by ATF (b), and area divisions on the reference image by ART (c) and by ATF (d)

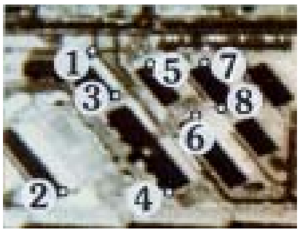

Fig. 8 Test points for performance evaluation

Table 1 Residual discrepancy $(\delta x, \delta y)$ [pixels]

Test Point	*by ART*		*by ATF*	
	IMG-B	IMG-C	IMG-B	IMG-C
1	(0, 0)	(0, 0)	(2, 1)	(6, 1)
2	(1, 0)	(1, 0)	(1, 0)	(3, 1)
3	(-1, -2)	(0, 1)	(4, 3)	(9, 3)
4	(1, 1)	(0, 0)	(2, 2)	(7, 0)
5	(-1, 0)	(0, 0)	(4, 3)	(8, 2)
6	(0, 0)	(1, 0)	(3, 4)	(5, 4)
7	(0, 1)	(0, 0)	(3, 3)	(5, 3)
8	(0, 0)	(0, 0)	(1, 4)	(2, 4)
Average	0.83	0.38	3.68	6.34

and 7 suggest us that ART removes both slight and severe discrepancy almost the perfectly, though ATF does not. Table 1 shows the numerical result, where residual discrepancy on test points (see Fig.8) are listed. As the mean residual discrepancy for both slightly and severely distorted images fall bellow 1 pixel, ART has enough performance in image registration.

In the simulation, ART generated 12 GCP pairs for IMG-B and 36 for IMG-C. This suggests ART generates new GCP pairs adaptively to degree of image distortion. ART took 166 seconds for processing IMG-B and 367 seconds for IMG-C, though ATF took less than 1 second for processing both images, where we used FACOM M780/10. The difference in the processing time seems to be large, but it it very time consuming process to taking GCP pairs manually. Considering the time to manually take many GCP pairs so that ATF achieves high accuracy as same as ART does automatically, ART has advantage in total performance.

5. ACTUAL IMAGE PROCESSING

We processed two airborne remote sensing images; one was acquired at 893 m in height and the other at 442 m as shown in Fig.9. Both images were acquired on the same day and almost the sage time. We used near infrared band ($0.8 \sim 0.9\mu m$) images with 256×256 pixels in size. The low altitude image was registered onto the high altitude image. Figures 10 show the registration results processed by ART and by ATF. We found that the result processed by ATF had large discrepancy but the discrepancy was removed by ART almost perfectly. Actually, ART generated 7 new GCPs so that they negated the spatial discrepancy. We also applied ART to another satellite remote sensing image pair. ART did not generate any GCP because both satellite images had no spatial discrepancy. This means ART works adaptively to the spatial discrepancy between the images to be registered and does not generate redundant GCP pair.

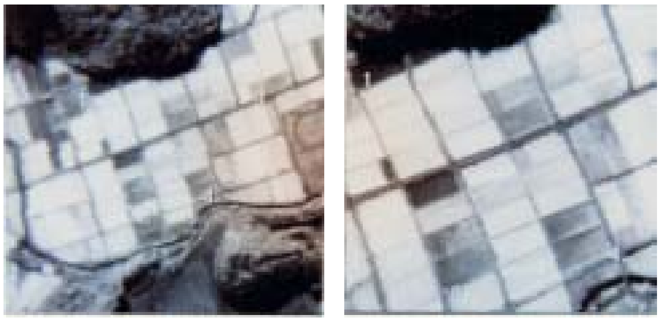

(a) (b)

Fig. 9 Actual remotely sensed images acquired at the height of 893 m (a) and 442 m (b)

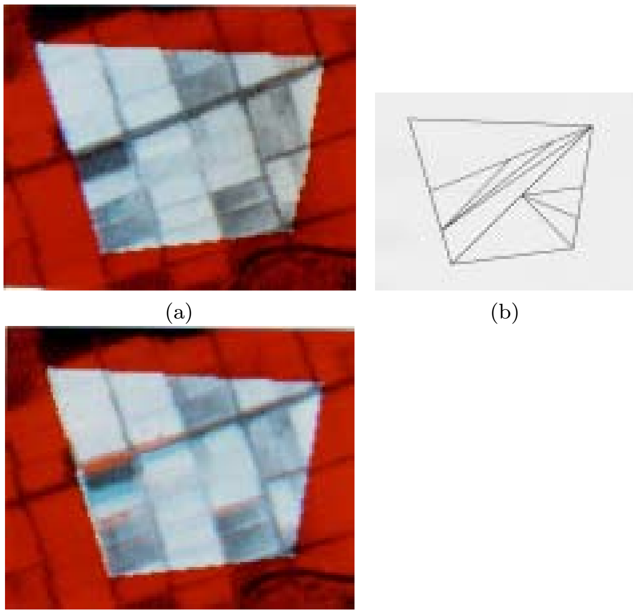

(a) (b) (c)

Fig. 10 Result processed by ART (a) and its area division (b) and result by ATF (c)

6. CONCLUSIONS

We proposed a registration technique ART which automatically generated new GCP pairs adaptively to the spatial discrepancy between images to be registered and achieved highly accurate registration as same as the conventional ATF did with many manually selected GCP pairs. The validity of ART was confirmed by numerical simulation and actual image processing. ART needed minimal number of initial GCP pairs to achieve highly accurate registration. As new GCP pair was generated adaptively to the spatial discrepancy, both inefficient processing for generating redundant GCP pairs and lack of accuracy due to less number of GCP pairs were not occurred.

To improve the performance by using multi-band data, to reduce processing time by adopting a segmentation technique, and to evaluate the effects of mis-selection of the initial GCP pairs are subjects for a future study.

References

1) P.E.Anuta : Spatial Registration of Multispectral and Multitemporal Digital Imagery Using Fast Fourier Transform Techniques, IEEE Trans., **GE**-8, 353/368 (1970)
2) D.I.Barnea and H.F.Silverman : A Class of Algorithms for Fast Digital Image Registration, IEEE Trans., **C**-21, 179/186 (1972)
3) W.F.Webber : Techniques for Image Registration, Proc. IEEE Conf. on Machine Processing of Remotely Sensed Data, 1B, 1/7 (1973)
4) R.A.Emmert and C.D.McGillem : Multitemporal Geometric Distortion Correction Utilizing the Affine Transformation, Proc. IEEE Conf. on Machine Processing of Remotely Sensed Data, 1B, 24/32 (1973)
5) M.Onoe, N.Maeda and M.Saito : Image Registration by Sequential Similarity Detection Algorithm, IPSJ Magazine 17-7, 634/640 (1976) (in Japanese)
6) N.Yoshida, Y.Yanagawa, S.Miwa and Y.Doi : Correction of Geometrical Distortion in Scanner Images, Proc. 5^{th} Remote Sensing Symposium (SICE), 61/62 (1979) (in Japanese)
7) K.Ohki, M.Inamura, H.Toyota and S.Fujimura : A Method for Registering Airborne Remote Sensing Images, Proc. 5^{th} Remote Sensing Symposium (SICE), 63/66 (1979) (in Japanese)
8) M.Onoe and M.Sone : Fast Image Registration based on Geometric Correspondence between Two Levels of Pyramid Structure, IEICE Trans. J70-D-1, 139/147 (1987) (in Japanese)
9) M.Takagi, T.Hiyama, M.Sone and M.Onoe : Automatic correcting Method of Geometric Distortion in Meteorological Satellite NOAA Image, IEICE Trans., J71-D-5, 883/893 (1988) (in Japanese)
10) M.Sone, S.Terada and M.Sakauchi : Fast Image Registration based on Feature Space and Pyramid Structure, IEICE Trans. J71-D-1, 102/109 (1988) (in Japanese)
11) A.Goshtasby : Registration of Images with Geometric Distortions, IEEE Trans., **GRS-26**-1, 60/64 (1988)
12) W.K.Pratt : Correction Techniques of Image Registration, IEEE Trans., **AES-10**, 353/358 (1974)
13) C.D.McGillem and M.Svedlow : Image Registration Error Variance as a Measure of Overlay Quality, IEEE Trans., **GE-14**, 44/49 (1976)
14) M.Seki, S.Fujimura and H.Mochizuki : Geometric Distortion Correction of Airborne Multispectral Scanner Data, SICE Trans., **18**-1, 64/70 (1982) (in Japanese)
15) Honma, Ihara, Furumura, Miyamoto and Kubo : Effects of Selection Quality of Ground Control Point Pairs on Accuracy of Correction of Geometric Distortion in Satellite Images, Proc. 3^{rd} Remote Sensing Symposium (SICE), 53/56 (1977) (in Japanese)
16) A.Goshtasby, G.C.Stockman and C.V.Page : a Regiion Based Approach to Digital Registration with Subpixel Accuracy, IEEE Trans., **GE-24**, 390/399 (1986)
17) W.A.Davis and s.K.Kenue : Automatic Selection of Control Points for the Registration of Digital Images, Proc. 4^{th} Int. Joint Conf. Pattern Recognition, 936/938 (1978)
18) H.Hanaizumi and H.Okumura : An Automatic Registration Method for Remotely Sensed Images, Proc. 14^{th} Remote Sensing Symposium (SICE), 101/104 (1988) (in Japanese)
19) H.Hanaizumi and H.Okumura : An Automatic Registration Method for Remotely Sensed Images (II) - Improvement of Searching for New Corresponding Control Points -, Proc. 28^{th} SICE Annual Conf., 139/140 (1989) (in Japanese)
20) H.Hanaizumi, H.Okumura, H.Tsubaki and S.Fujimura : An Automatic Registration Method for Remotely Sensed Multispectral Images by Using Spatial Correlation between Local Triangles, Proc. IGARSS'89, 1287/1290 (1989)
21) H.Hanaizumi, H.Okumura, H.Tsubaki and S.Fujimura : An Automatic Registration Method for Remotely Sensed Images by Using Spatial Correlation between Local Triangles, SICE Trans., **28**-1, 168/169 (1992) (in Japanese)
22) S.Fujimura and H.Hanaizumi : Hierarchical Algorithms for the Classification of Remotely Sensed Multi-Spectral Images, IEICE Trans., **E-74**-2, 295/301 (1991)

Hiroshi Hanaizumi (Member)

received the B.Sc. degree in communication engineering from the University of Electro-Communications, Tokyo, Japan, in 1978, and the M. Eng. and Dr.Eng. degrees in mathematical engineering and instrumentation physics from The University of Tokyo, in 1980 and 1987, respectively.
He is currently a Professor in the Department of Digital Media Science in Hosei University. His current research interests are image processing and remote sensing.
Dr. Hanaizumi is a member of the Institute of Electrical and Electronics Engineers, Institute of Electronics, Information and Communication Engineers, among others.

Hiroshi Okumura (Member)

received the B.E. and M.E. degrees in systems engineering from Hosei University in 1988 and 1990, respectively, and Ph.D. degree in environmental science from Chiba University in 1993.
He is currently a Associate Professor in the Department of Information Science in Saga University. His research interests are human visual perception, image processing, pattern recognition and remote sensing. Dr. Okumura is a member of the Institute of Electronics, Information and Communication Engineers and so forth.

Hiroe Tsubaki (Member)

received the B. Eng., M. Eng. and Dr. Eng. degrees in mathematical engineering and information physics from The University of Tokyo, in 1980, 1982 and 1988, respectively.
He is currently a Professor in the Graduate School of Business Sciences, University of Tsukuba. His current research interests are applied statistics, quality control, and so on.
Dr. Tsubaki is a member of Applied Statistics Society of Japan, Biometric Society, and Japanese Society for Quality Control.

Sadao Fujimura (Member)

received the B. Sc., M. Sc., and Ph. D degrees in applied physics from the University of Tokyo, Tokyo, Japan in 1963, 1965 and 1968, respectively. He is currently a Professor at the Department of Information Engineering Faculty of Informatics, Teikyo Heisei University, Ichihara, Japan. He served as a lecturer in the same department from 1968 to 1973. After that he joined the University of Electro-Communications, Tokyo, as an associate professor, and in 1978 rejoined the Department above of the University of Tokyo, and served as professor there from 1980 to 2000. He joined the present university from 2000. He was a visiting professor at the Department of Electric Engineering, University of Tennessee, Knoxville, Tennessee. His research interests are in image processing, especially multi-dimensional image processing, pattern recognition, infrared thermometry, remote sensing and 3D distribution and shape measurement. He is a fellow of the Society of Instrument and Control Engineers, and a sinior member of IEEE, a member of SPIE, the Japan Society of Applied Physics, the Institute of Electric Engineering and so forth.

Rewrited from T.SICE Vol.31,No.6,685/691(1995)